

## **Rational designs of polypropylene composite foam with open-cell structure via graphite conductive network for sound absorption**

Zhiyao Li<sup>1</sup>, Chenguang Yang<sup>1,3,\*</sup>, Kun Yan<sup>1</sup>, Ming Xia<sup>1</sup>, Zhong Yan<sup>1</sup>, Dong Wang<sup>1,2\*</sup>, Wenwen Wang<sup>1</sup>,

\*

<sup>1</sup> Key Laboratory of Textile Fiber and Products (Wuhan Textile University), Ministry of Education, Wuhan Textile University, Wuhan 430200, China

<sup>2</sup> College of Chemistry, Chemical Engineering and Biotechnology, Donghua University, Shanghai 201620, China

<sup>3</sup> Hubei Key Laboratory of Plasma Chemistry and Advanced Materials, Wuhan Institute of Technology, Wuhan 430205, China

\*Corresponding author. E-mail address: cgyang@wtu.edu.cn; wangdon08@126.com;

wwang@wtu.edu.cn.

# 1. Materials and Experimental Procedures

## 1.1. Materials

Isotactic polypropylene T03 (iPP, pellets) was purchased from Sinopec Shanghai Chemical Co (Shanghai, China). The graphite powder (Lgshimo, 160 nm, Fig. S1a, b) was purchased from Liugong Graphite Co., LTD (Zhengzhou, China).

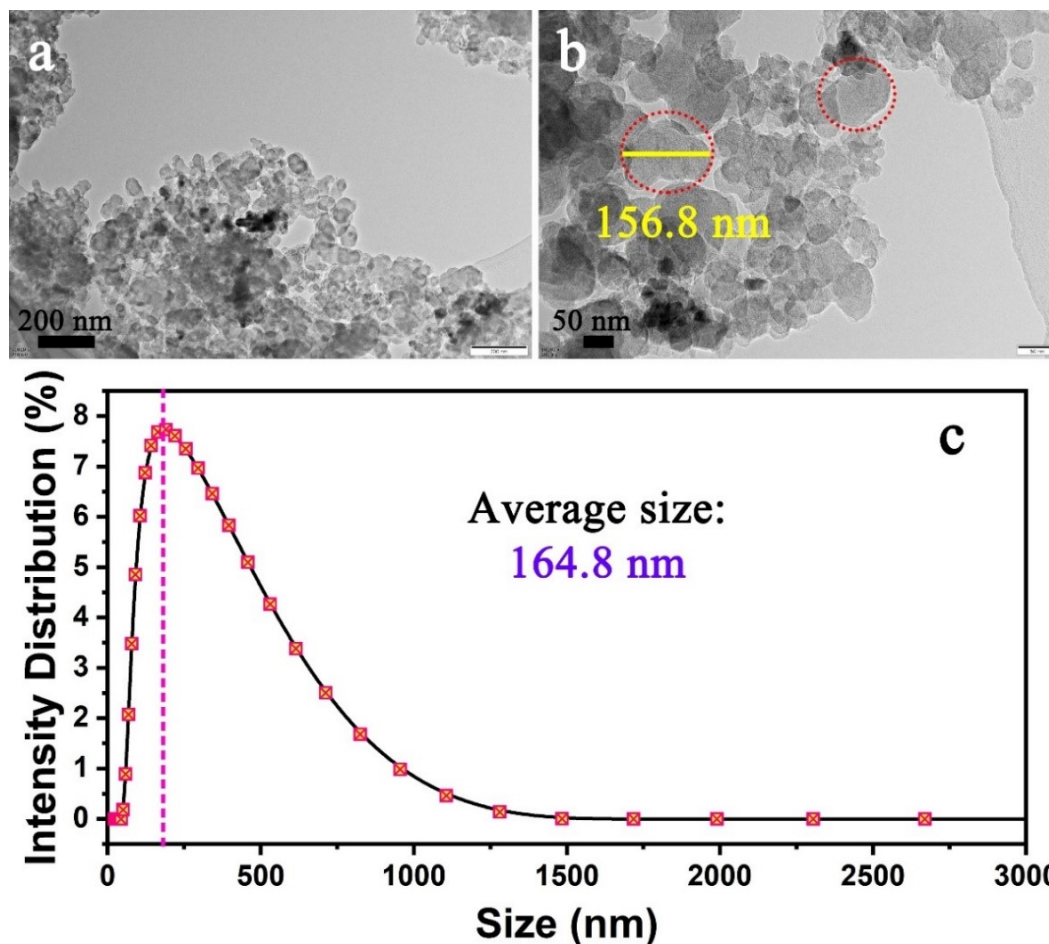


Fig. S1 SEM high magnification image (a), low magnification image (b), and size distribution of the graphite particles (c)

## 1.2. Sample preparation

Table S1. Foaming conditions of pure PP and PP-G samples

Sample weight (g)	Temperature (°C)	Saturation pressure (MPa)	Saturation time (h)
9	152	30	3.5

## 1.3. Sample characterization

### Cell morphology characterization

The pressure relief rate of different foaming substrates under the same pressure and temperature is measured by the sensor on the foaming equipment.

The foam morphology was observed using a scanning electron microscope (SEM; JEOL JSM-IT300, Japan). Image-Pro Plus 6.0 software was used to analyze the SEM photographs. The surface plot model of the samples was also simulated by Image-Pro Plus 6.0, which more intuitively reflects the structure of the materials. The average diameter  $D$  of the cells in the micrographs was calculated using Eq. (S1) <sup>1</sup>.

$$D = \frac{\sum d_i n_i}{\sum n_i} \quad (\text{S1})$$

where  $n_i$  is the number of cells with a perimeter-equivalent diameter of  $d_i$ . To ensure the accuracy of the average pore size measurement,  $i$  is greater than 150.

The volume expansion ratio of each sample was calculated as the ratio of the density of the original sample,  $\rho_s$ , to the measured density of the foam sample,  $\rho_f$ . The densities ( $\rho_f$ ) of the foam samples were determined from Archimedes' law by weighing the polymer foam in water with a sinker using an electronic analytical balance (HANG-PING FA2104) and using Eq. (S2) to calculate the density.

$$\rho_f = \left( \frac{a}{a + b - c} \right) \rho_w \quad (\text{S2})$$

where  $a$ ,  $b$ , and  $c$  are the weights of the specimen in air without the sinker, the totally immersed sinker, and the specimen immersed in water with the sinker, respectively, and  $\rho_w$  is the density of water.

The volume expansion ratio ( $V_f$ ) was calculated using Eq. (S3).

$$V_f = \frac{\rho_s}{\rho_f} \quad (\text{S3})$$

where  $\rho_s$  and  $\rho_f$  are the density of solid and foam samples, respectively.

The cell density ( $N$ ) was determined as the number of cells per unit volume of the foam, which was calculated using Eq. (S4).

$$N_0 = \left( \frac{n}{A} \right)^{3/2} V_f \quad (\text{S4})$$

where  $n$  and  $A$  are the numbers of cells in the micrograph and the area of the micrograph ( $\text{cm}^2$ ), respectively.

The open-cell content was measured by an automatic true density meter (AccuPyc II 1340) in accordance with ISO4590. According to the principle of gas displacement, the open cell ratio of the foamed samples was tested. The number of tests was 5, and the test was stopped when the error was less

than 0.01%. The open-cell content was obtained from the average of the last 5 measurements.

TGA was performed to evaluate the thermal stability of the stability of the unfoamed neat PP, PP-G, and foamed PP-G samples using a Thermogravimetric Analyzer (NETZSCH, TG 209 F3 Tarsus) from 50 to 800 °C with a heating rate of 10 °C/min and nitrogen flow of 20 mL/min.

#### **Thermal conductivity test**

The thermal conductivity of solid and foam samples was measured by a laser thermal conductivity measuring instrument (LFA427, Netzsch) in accordance with GB/T 10294-2008.

#### **Sound absorption test**

An impedance tube device (BSWA SW260, BSWA Technology Co., Ltd.) was used to measure the change of the sound absorption coefficient following the ISO standard (ISO10534-2) based on the transfer function method. The absorption coefficient is defined as the ratio of the acoustic energy absorbed by a sample (incident–reflected) to the incident acoustic energy (incident) as a function of frequency. Six measurements were performed for each sample in the frequency range from 0 to 6000 Hz with two 1/4 in microphones and the frequencies selected were 1000, 2000, 4000, and 6000 Hz, respectively.

#### **Tortuosity test**

The foam is immersed in a CaSO<sub>4</sub> conductive solution, and the voltage measures the resistivity ( $R_c$ ) and the current between the two copper electrodes. The tortuosity  $T$  is calculated by the following Eq. (S5).

$$T = p \left( \frac{R_c}{R_f} \right) \quad (S5)$$

Where:  $R_f$  is the resistivity of the measured fluid, the measured voltage is 0-1.5 V;  $P$  is the porosity, %<sup>2</sup>.

#### **Cyclic compression performance**

The compression test was performed on a universal testing machine (Instron 5967, Boston, USA) according to ISO 844:2004. A cube sample with a side length of 20 mm was cut from the foam. The compression speed is 5.0 mm/min (5, 20, and 50 cycles), and the maximum deformation is 80 %.

#### **Wettability characterization**

An at tension theta system (KSV Instruments Ltd., Finland) was used to evaluate the hydrophobic of the samples.

### **1.4. Optimization model design**

A typical square root optimization model (Eq. S6) is used in this work.

$$y' = \sqrt{y + k} \quad (S6)$$

The process sequence is executed according to the main effect. The optimal design software Design-Expert 12.0 was used to obtain the final equation (Eq. S7) according to the actual factors.

$$\begin{aligned} \text{Sqrt}(\text{Flow resistance}) = & 2.73877 + 0.010456 \times \text{cell size} + 2.15803 \times \text{tortuosity} - \\ & 0.014209 \times \text{cell size} \times \text{tortuosity} \end{aligned} \quad (S7)$$

## 2. Results and Discussion

### 2.1. Cell size distribution

In Fig. S2, the cell size distribution peak of the foamed materials with different component ratios moved to the direction of size reduction and the distribution peak width narrowed with the increased loading amount of graphite powder. This indicated that the nano-graphite particles enhanced the heterogeneous nucleation during foaming process. With the increased number of micronuclei, the competition mechanism between micronucleus was significantly enhanced for limited CO<sub>2</sub>, and the cell size significantly decreased.

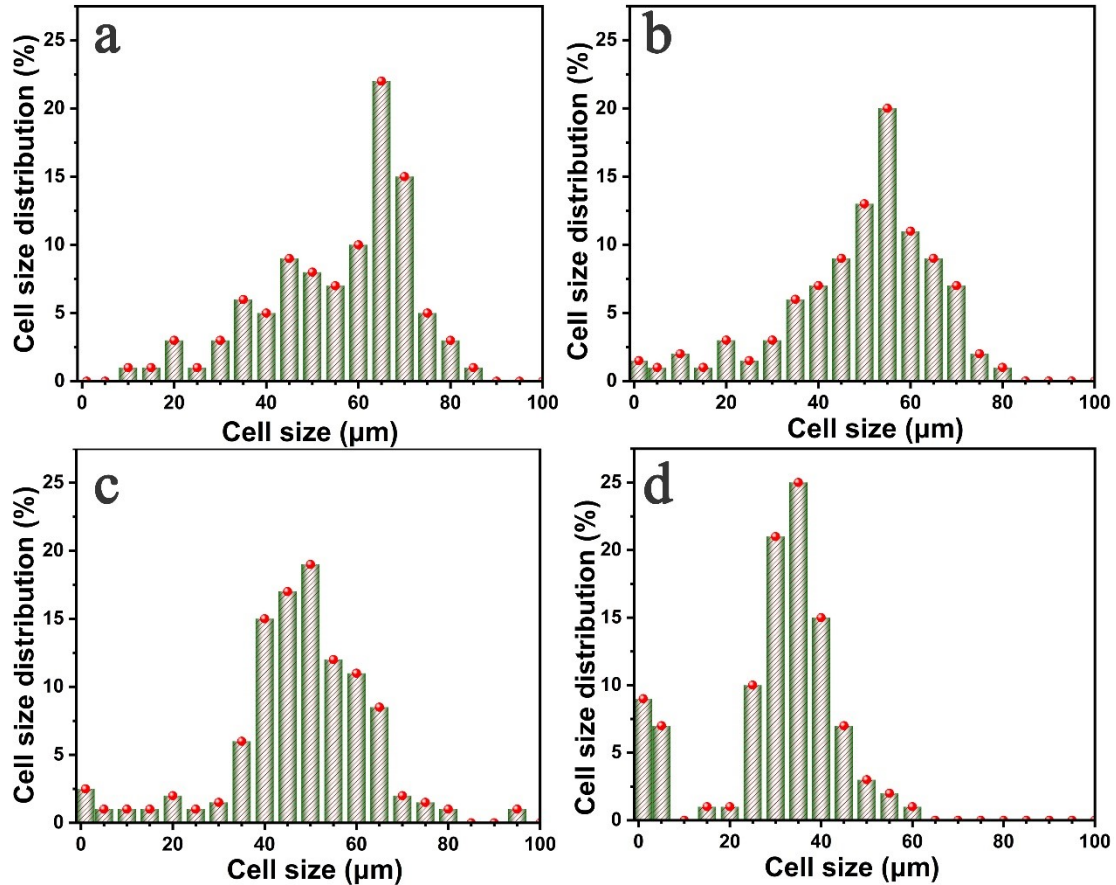


Fig. S2 Cell size distributions of different foams with different amounts of nano-graphite powder: PP (a), PP-G(1.0) (b), PP-G(5.0) (c), and PP-G(10.0) (d)

## 2.2. Foam density of the foams

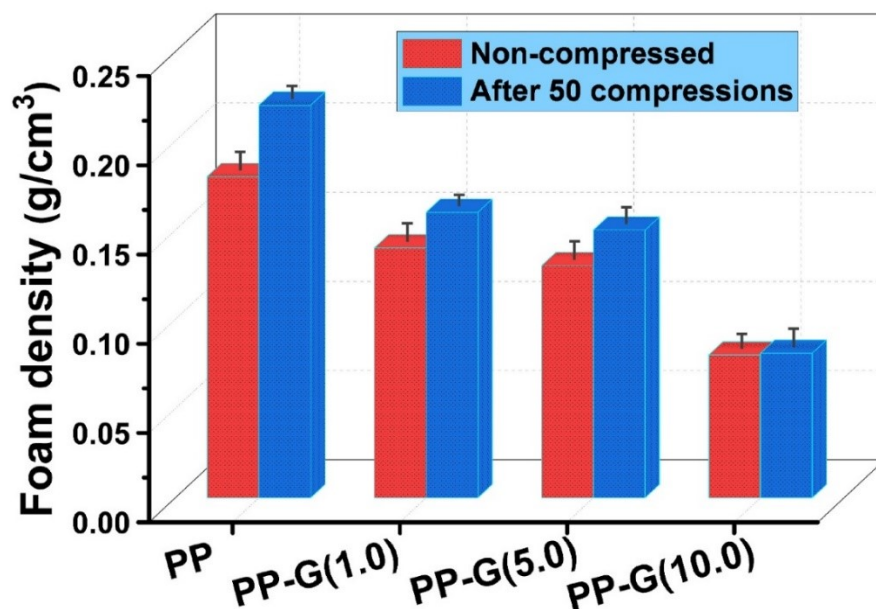
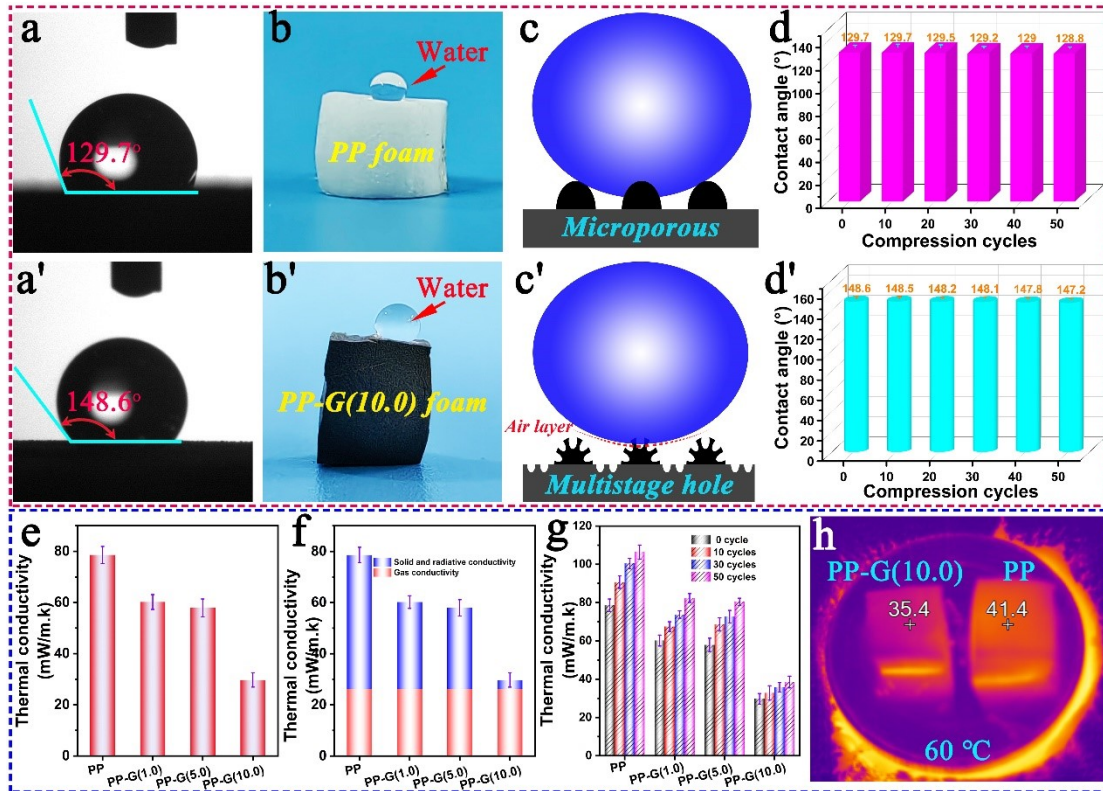


Fig. S3. Density changes of different foams before and after 50 cycles of compression

## 2.3. Hydrophobic and thermal insulation properties

In Fig. S4a and a', the water contact angle of the PP-G(10.0) foam is  $148.6^\circ$ , which is almost superhydrophobic, and the digital photos can be seen in Fig. S4b and b'. The excellent hydrophobic performance was mainly attributed to the micro/nano porous structure of its cross section, which made it easier to form air layer between water droplets and the material interface (Fig. S4c and c'). Then, we compared the change of water contact angle of foams after repeated compression, as shown in Fig. S4d and d'. The water contact angles of the two foams changed little after repeated compression, which is related to the excellent mechanical property of PP itself.



**Fig.S4** Water contact angle (a) and (a'), images of water droplet attached foam materials (b) and (b'), hydrophobic mechanism of two foams (c) and (c'), change of water contact angle of two foaming materials after cyclic compression (d) and (d'), different foam thermal conductivity (e), different heat transfer contribution ratios (f), thermal conductivity after multiple cycle compression (g), and comparison of surface temperatures of different foams (h)

Fig. S4e, f, g, and h are the thermal conductivity of different foams. In Fig. S4e, the thermal conductivities decreased greatly as the graphite particles load increasing and the thermal conductivity declined to 29.6 mW/m·K when the graphite's added amount is 10 wt%. The air thermal conductivity is 26.3 mW/m·K<sup>3</sup>, so for PP-G(10.0) foam, the sum of solid and radiation conduction contribution values is 3.3 mW/m·K, and the solid conduction contribution rate is only 12.5%. The excellent thermal insulation performance is attributed to the high expansion rate of the composite foam, which greatly increases the heat transfer path and significantly decreases the heat transfer coefficient. The PP-G(10.0) composite foam prepared in this work also has excellent thermal insulation performance, which is attributed to the high porosity of the composite foam.

## References

1. J. Zhao, G. Wang, C. Wang and C. B. Park, *Composites Science and Technology*, 2020, **191**, 108084.
2. M. Álvarez-Láinez, M. A. Rodríguez-Pérez and J. A. de Saja, *Materials Letters*, 2014, **121**, 26-30.
3. R. A. Campo-Arnáiz, M. A. Rodríguez-Pérez, B. Calvo and J. A. de Saja, *Journal of Polymer Science Part B: Polymer Physics*, 2005, **43**, 1608-1617.